Unstructured to structured transition of an intrinsically disordered protein peptide in coupling Ca^{2+}-sensing and SK channel activation

Miao Zhang[a], John M. Pascal[b], and Ji-Fang Zhang[a,c,d,1]

Departments of [a]Molecular Physiology and Biophysics and [b]Biochemistry and Molecular Biology, [c]Farber Institute for Neurosciences, and [d]Graduate Program in Neuroscience, Thomas Jefferson University, Philadelphia, PA 19107

Edited by Richard W. Aldrich, University of Texas at Austin, Austin, TX, and approved February 7, 2013 (received for review November 21, 2012)

Most proteins, such as ion channels, form well-organized 3D structures to carry out their specific functions. A typical voltage-gated potassium channel subunit has six transmembrane segments (S1–S6) to form the voltage-sensing domain and the pore domain. Conformational changes of these domains result in opening of the channel pore. Intrinsically disordered (ID) proteins/peptides are considered equally important for the protein functions. However, it is difficult to explore the structural features underlying the functions of ID proteins/peptides by conventional methods, such as X-ray crystallography, because of the flexibility of their secondary structures. Unlike voltage-gated potassium channels, families of small- and intermediate-conductance Ca^{2+}-activated potassium (SK/IK) channels with important roles in regulating membrane excitability are activated exclusively by Ca^{2+}-bound calmodulin (CaM). Upon binding of Ca^{2+} to CaM, a 2 × 2 structure forms between CaM and the CaM-binding domain. A channel fragment that connects S6 and the CaM-binding domain is not visible in the protein crystal structure, suggesting that this fragment is an ID fragment. Here we show that the conformation of the ID fragment in SK channels becomes readily identifiable in the presence of NS309, the most potent compound that potentiates the channel activities. This well-defined conformation of the ID fragment, stabilized by NS309, increases the channel open probability at a given Ca^{2+} concentration. Our results demonstrate that the ID fragment, itself a target for drugs modulating SK channel activities, plays a unique role in coupling Ca^{2+} sensing by CaM and mechanical opening of SK channels.

calcium | signaling | gating

Most proteins typically adopt one or more well-defined 3D structures, or domains, to carry out their specific functions. Voltage-gated potassium channels are such an example, with six transmembrane segments (S1–S6) forming the voltage-sensing domain and the pore domain (1, 2). Conformational changes of these domains result in opening of the channel pore. Unlike the well-structured proteins, there are proteins or fragments of proteins that lack well-defined 3D conformations (3–8). These proteins, termed "intrinsically disordered" (ID) proteins/peptides, typically are flexible in their secondary structures and often can adopt multiple conformations. Consequently, the structures of ID proteins are difficult to determine by conventional methods, such as X-ray crystallography, and it is difficult to explore the structural features responsible for functions by ID proteins. Nevertheless, emerging evidence shows that ID proteins/peptides are equally important for the protein functions.

Small- and intermediate-conductance Ca^{2+}-activated K^+ (SK/IK) channels play important roles in regulating membrane excitability by Ca^{2+} (9–13). SK and IK channels belong to the same gene family, with four genes identified: KCNN1 for KCa2.1 channels (SK1), KCNN2 for KCa2.2 (SK2), KCNN3 for KCa2.3 (SK3), and KCNN4 for KCa3.1 (IK) (11, 13). We recently identified a functional SK2 channel splice variant, SK2-b, which is less sensitive to Ca^{2+} for its activation (14). By dampening the firing of action potentials, activation of SK/IK channels contributes to the regulation of neuronal excitability, dendritic integration, synaptic transmission, and plasticity in the central nervous system (9, 11, 13, 15, 16). In the cardiovascular system, vascular endothelial cells express both IK and SK3 channels, which are implicated in the endothelium-derived hyperpolarizing factor–mediated vasodilation (17–20). The importance of SK/IK channels is demonstrated further by their potential roles in clinical abnormalities (21–24). SNPs in the SK/IK genes are thought to play a role in cardiovascular abnormalities, such as familial atrial fibrillation (22, 25). Compromised SK channel activities may be a contributing factor of hypertension (21). Activation of SK channels in the nucleus accumbens region of the brain could help treat alcohol addiction (26). Administration of positive SK channel modulators is beneficial in animal models of neurodegenerative diseases, such as ataxia (27). Given the roles of SK/IK channels in physiological and pathophysiological conditions, a tremendous amount of effort has been devoted to developing small molecules targeting SK/IK channels including such compounds as 1-ethyl-2-benzimidazolinone (1-EBIO) and NS309 (15, 28–32). Although 1-EBIO is the prototype of these compounds, NS309 is the most potent one. Some of these compounds, such as chlorzoxazone and riluzole (Rilutek), have been used in multiple clinical trials for neurological disorders, such as alcoholism and cerebella ataxia (http://clinicaltrials.gov). However, it has not been known how these compounds, such as NS309, achieve their effects in potentiating SK/IK channels.

Like voltage-gated potassium channels, SK/IK channels are tetramers, and each subunit consists of six transmembrane segments. However, SK/IK channels are activated exclusively by Ca^{2+}-bound calmodulin (CaM) tethered to the channel C terminus (33, 34). CaM serves as the high-affinity Ca^{2+} sensor, with four canonical EF hands, two located at the CaM N terminus (N-lobe) and the other two at the C terminus (C-lobe) (35). The CaM N- and C-lobes are connected by the CaM linker. Binding of Ca^{2+} to CaM causes significant changes in the conformations of both CaM and the CaM binding domain (CaMBD), leading to the formation of a 2 × 2 complex between CaM and the CaMBD (14, 36, 37). A channel fragment, R396–M412, which connects S6 and the CaMBD, is not visible in the protein crystal structure, indicating that this fragment is an intrinsically disordered fragment (IDF). Although Ca^{2+}-dependent formation of this 2 × 2 complex is a critical initial step for Ca^{2+}-dependent activation of SK channels, it is not clear how the binding of Ca^{2+} to CaM is coupled to the eventual opening of the SK channel.

Here we show that the conformation of the IDF becomes clearly identifiable from the protein crystals of CaM–CaMBD complexed with NS309, a potent positive channel modulator (38, 39). In the

Author contributions: M.Z., J.M.P., and J.-F.Z. designed research, performed research, analyzed data, and wrote the paper.

The authors declare no conflict of interest.

This article is a PNAS Direct Submission.

Data deposition: Crystallography, atomic coordinates, and structure factors have been deposited in the Protein Data Bank, www.pdb.org (PDB ID code 4J9Y and 4J9Z).

[1]To whom correspondence should be addressed. E-mail: Ji-Fang.Zhang@jefferson.edu.

This article contains supporting information online at www.pnas.org/lookup/suppl/doi:10.1073/pnas.1220253110/-/DCSupplemental.

structures, both ends of the IDF are anchored to CaM with or without NS309. Binding of NS309 results in the transition of the unstructured IDF to a well-defined structure. This distinctive IDF conformation, stabilized by binding of NS309 or cross-linking A477 of the CaMBD and F410 of the IDF, increases the channel open probability at a given Ca^{2+} concentration. Our results demonstrate that the IDF plays a unique role in coupling binding of Ca^{2+} to CaM and the mechanical opening of SK channels. The results further show that the IDF is the target for compounds, such as NS309, thus providing a rationale for development of small-molecule compounds targeting ID proteins (3, 40).

Results

Interaction Between CaM and the CaMBD at the CaM Linker Region. A previous report shows that the channel fragment, R396–M412, which connects S6 and the CaMBD, is not visible in the structure of the CaM–CaMBD2-a complex (Fig. S1*A*) (37). Sequence alignment shows that this fragment is highly conserved in SK channels, from *Drosophila* to human, as well as among all four subfamilies of SK channels, including SK1, SK2, SK3, and IK (Fig. 1*A*). Our determination of the structure of the CaM–CaMBD2-a complex from multiple sets of X-ray diffraction data (at the resolution of 1.5–1.7 Å; Table S1, PDB code 4J9Y) consistently shows the interaction between the CaM linker region and E39–K402 of the missing channel fragment (Fig. 1*B* and Fig. S1*B*) instead of the previously reported interaction between the CaM linker region and the polyhistidine tag used to purify the CaMBD (Fig. S1*A*) (37).

Fig. 1*C* shows the electron density map with the refined structure coordinates for amino acid residues E399, L400, T401, and K402 at the CaM linker region (near D78 and T79 of CaM, at 1.54 Å) superimposed. Assigning these four amino acid residues yields a much better representation of the electron density map in that region than the polyhistidines (Fig. 1*C* and Fig. S1 *C* and *D*). These four amino acid residues wrap around the CaM linker region and form a cuff-like structure (Fig. 1*D*) that interacts with the following amino acid residues from CaM: K75, K77, D78, T79, D80, S81, and E84 (within the 5-Å radius of the cuff residues; Fig. 1*D*). Among these CaM residues, D78 and T79 interact with all four cuff residues. Analysis further shows that T79, but not D78, interacts only with these four cuff residues (within the 5-Å radius).

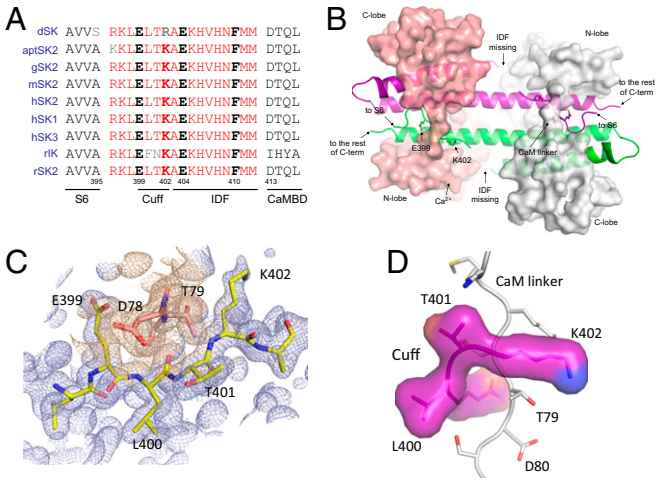

Fig. 1. Structure of the channel cuff (E399–K402) and its interaction with the CaM linker. (*A*) Alignment of the amino acid sequences R396–M412 of SK channels from different species, *Drosophila* to human, plus the sequence of the rat IK channel. This fragment, including the cuff and the IDF, is highly conserved. D, *Drosophila*; apt, Apteronotus; g, chicken; m, mouse, h, human; r, rat. Numbering is based on the rSK2-a sequence. The only differences between IK and SK channels in this region are F and N at the equivalent positions of L400 and T401 of the rSK2-a sequence. (*B*) Structure of the entire 2 × 2 CaM–CaMBD2-a complex. The surface models represent CaM (salmon and gray), and the cartoon represents the channel fragment (green and purple). The structure was determined from protein crystals in the presence of Ca^{2+} but without NS309. Note that the structure of the IDF is not identifiable. (*C*) Electron density map of the channel cuff (light blue) and the CaM linker (D78 and T79, wheat) constructed using 2mFo–DFc coefficients calculated in PHENIX. The map is contoured at 1.0 σ and is overlaid with coordinates from the current, refined model for the cuff residues (yellow sticks) and D78 and T79 of CaM (salmon sticks). (*D*) The interaction between the channel cuff and the CaM linker (gray, vertical). T79 of CaM is located closed to K402 of the cuff.

Cuff–Linker Interaction on Ca^{2+}-Dependent Channel Activation. Because it was not known whether the interaction between the CaM linker and the target proteins has functional consequences, we sought to determine whether the interaction between the channel cuff and the CaM linker region might affect the Ca^{2+}-dependent activation of the SK channel. From the structural data (Fig. 1), mutations were made in selected amino acid residues from both the channel cuff and the CaM linker, and their effects on Ca^{2+}-dependent channel activation were tested using inside-out patches. Compared with WT SK2-a ($EC_{50} = 0.32 \pm 0.03$ μM, $n = 8$), both L400A and E400A become less responsive to Ca^{2+} for their activation, with the EC_{50}s at 0.69 ± 0.14 μM ($n = 5$, $P = 0.007$) and 0.47 ± 0.02 μM ($n = 4$, $P = 0.023$, respectively (Fig. 2*A*). T401A, on the other hand, does not change its Ca^{2+}-dependent channel activation significantly ($EC_{50} = 0.27 \pm 0.03$ μM, $n = 3$, $P = 0.346$). Although T79 of CaM interacts directly with all four cuff residues, it is located closer to K402 (Fig. 1*D*). Therefore we tested whether changes in the polarity of T79 of CaM might affect Ca^{2+}-dependent channel activation.

A mutant CaM, T79C, was created to take advantage of (*i*) the lack of cysteine residues in CaM and the presence of only one cysteine residue, C3, located at the channel N terminus on the channel cytoplasmic side and (*ii*) methanethiosulfonate (MTS) reagents that can modify the cysteine residue directly during experiments (41). When coexpressed with SK2-a (WT), the T79C mutation itself does not alter the Ca^{2+}-dependent channel activation ($EC_{50} = 0.35 \pm 0.02$ μM, $n = 3$, Fig. 2*C*), nor does application of methyl methanethiosulfonate (MMTS, neutral, 2 mM, $EC_{50} = 0.33 \pm 0.008$ μM, $n = 3$, Fig. 2C). However, charged MTS reagents, such as 2-sulfonatoethyl methanethiosulfonate (MTSES, a negative charge, 2 mM) and 2-(trimethylammonium)ethyl methanethiosulfonate (MTSET, a positive charge, 2 mM), rapidly reduce the current amplitude (Fig. 2*B* and Fig. S2*B*), resulting in significant shifts of Ca^{2+}-dependent channel activation to the right, with EC_{50}s at 0.76 ± 0.08 μM ($n = 4$, $P = 0.007$) and 0.92 ± 0.03 μM ($n = 3$, $P = 0.001$), respectively (Fig. 2*C*). Control experiments using SK2-a coexpressed with WT CaM show that MTSES (2 mM) or MTSET (2 mM) has no impact on Ca^{2+}-dependent channel activation, with the EC_{50} at 0.35 ± 0.002 μM ($n = 3$) or 0.36 ± 0.04 μM ($n = 4$), respectively (Fig. S2*A* and Fig. 2*C*). The effects of charges at CaM T79 are confirmed further by the CaM mutants T79D and T79K, both of which become significantly less responsive to Ca^{2+} for their activation ($EC_{50} = 1.19 \pm 0.19$ μM, $n = 4$, and 2.48 ± 0.25 μM, $n = 3$, respectively) (Fig. S2*C*).

Although results from these mutants indicate that the channel cuff and the CaM linker are involved in Ca^{2+}-dependent channel activation, shifts in the dose–response curves by these mutations are not necessarily the consequence of disruption of the interaction between the channel cuff and the CaM linker. We next used mutant cycle analysis to address this causal relationship, independent of our structural data. If there is no direct interaction between the channel cuff and the CaM linker, the coupling coefficient, Ω, will be unity (42, 43). Based on the structural data, the SK2-a:CaM pairs WT:WT, E399Q/K402L:WT, WT:T79D, and E399Q/K402L:T79D were expressed in TsA cells, and their Ca^{2+}-dependent activation was determined. The EC_{50}s are 0.32 ± 0.03 μM ($n = 8$), 0.77 ± 0.06 μM ($n = 3$), 1.19 ± 0.19 μM ($n = 4$), and 1.02 ± 0.07 μM ($n = 3$), respectively. There are no significant differences in changes of the Gibbs free energy (ΔΔG) among the three mutants (Fig. 2*D*), indicating the direct interaction between the channel cuff and the CaM linker. Most importantly,

PHYSIOLOGY

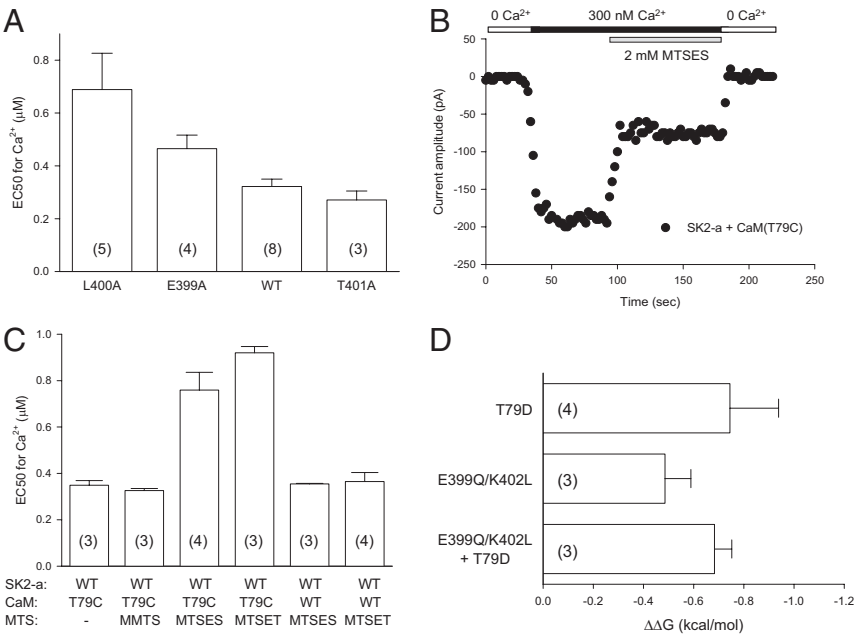

Fig. 2. Effects of the cuff–CaM linker interaction on SK channel activation. (*A*) L400A and E399A mutants become less responsive to Ca^{2+} for their activation, but T401A does not produce significant changes in its Ca^{2+}-dependent activation. Values in parentheses indicate the number of experiments. (*B*) Application of MTSES to T79C reduces the SK channel current amplitude. (*C*) Effects of T79C (CaM) and application of MTS reagents on Ca^{2+}-dependent channel activation. MMTS, MTSES, or MTSET was mixed in the bath solution with 300 nM Ca^{2+} just before their application during recording. (*D*) Changes in Gibbs free energy (ΔΔG) for the CaM:SK2-a pairs T79D:WT, WT:E399Q/K402L, and T79D:E399Q/K402L. No statistical differences were found for ΔΔG among the three pairs, suggesting the direct interaction between the CaM linker and the channel cuff.

the coupling coefficient, Ω, is 2.81 ± 1.28 (mean ± SD), which is significantly larger than 1 ($P < 0.03$), demonstrating unequivocally that the channel cuff (E399–K402) interacts directly with the CaM linker region, particularly T79. Disruption of such interactions by mutations causes shifts in Ca^{2+}-dependent activation of these mutants. Furthermore, the interaction between the channel cuff and CaM linker means that both N- and C-terminal ends of the IDF are anchored to CaM in the intact and functional channel, even though our structural data were obtained from the channel fragment (Fig. 1*B*).

Structure of the NS309 Binding Site. We next tested the potential functions of the IDF, A403–M412 (Fig. 1*A*). The structure of the IDF is not identifiable in the protein complex regardless whether the protein crystals are obtained in the presence of Ca^{2+} (Fig. 1*B*) or not (36). Attempts were made to crystallize the CaM–CaMBD2-a complex associated with NS309, the most potent positive modulator of SK/IK channels (38, 39). By soaking the naive crystals of CaM–CaMBD2-a in solution with the saturating concentration of NS309 for a prolonged period, we successfully determined the structure of the NS309-bound protein complex at the resolution of 1.7 Å (Fig. 3, Fig. S3, and Table S1, PDB code 4J9Z). The NS309 binding site is located at the interface between the CaM N-lobe and the CaMBD (Fig. 3*A* and Fig. S3*A*), similar to that of 1-EBIO (44). The most striking and unexpected feature of the NS309-bound CaM–CaMBD2-a structure is the appearance of the structure of the IDF (Fig. 3 *B* and *C* and Fig. S3 *B–F*, compare with Fig. 1*B*). The appearance of the IDF structure has led to additional contact points between CaM and the channel, such as the formation of a salt bridge between E404 of the IDF and K75 of CaM at the CaM linker (Fig. 3*B* and Fig. S4*A*). Without NS309, the structure of the E404 side chain cannot be determined beyond the β-carbon. The NS309 binding site has unique structural features that may account for its high potency (Fig. S4 *B* and *C*). For instance, the location of the benzene ring of NS309 differs from that of 1-EBIO (Fig. S4*B*). Most notably, NS309 forms contacts with F410 of the IDF (Fig. 3 *A* and *B*). To verify the functional interaction between NS309 and F410 of the IDF, mutations at F410 were introduced, and their responses to the application of NS309 were determined. Shown in Fig. 3*D* are the results of the F410L mutation, which significantly decreases the potency of NS309, with the EC_{50} increased from 0.44 ± 0.14 μM ($n = 3$) to 1.79 ± 0.24 μM ($n = 5$, $P = 0.007$). The F410L mutation does not have any impact on its Ca^{2+}-dependent activation (EC_{50} = 0.34 ± 0.03 μM, $n = 4$) (Fig. S4*D*).

Unique Role of the IDF in Ca^{2+}-Dependent Activation of SK Channels. NS309 potentiates the channel activity by increasing the channel open probability at a given Ca^{2+} concentration. In the presence of 3 μM NS309, the EC_{50} for Ca^{2+}-dependent channel activation is reduced to 0.054 ± 0.002 μM ($n = 3$, $P < 0.001$; Fig. 4*A*).

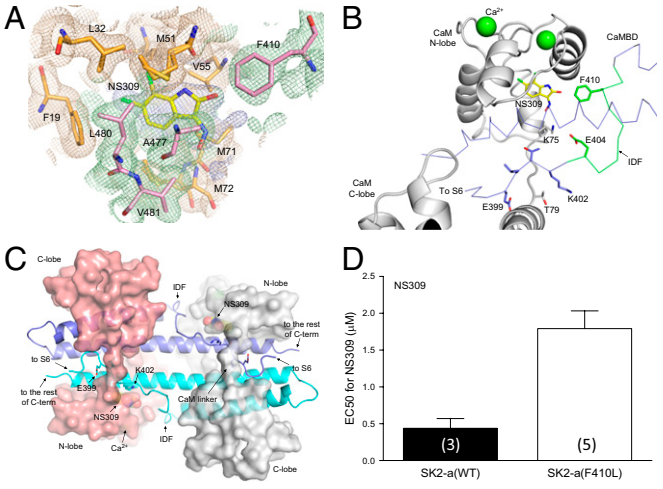

Fig. 3. Transition of the IDF conformation from unstructured to structured in the presence of NS309, a potent channel modulator. (*A*) Electron density map (light blue) shows the presence of additional electron density at the interface between CaM (wheat) and the CaMBD (pale green) at the CaM N-lobe. The map is contoured at 0.5 σ and is overlaid with the current refined coordinates for NS309 and amino acid residues from CaM (orange) and the CaMBD (pink) that surround NS309. (*B*) F410 from the IDF is part of the NS309 binding pocket. The distance between F410 and NS309 is 3.4 Å. Note the appearance of the IDF at a different viewing angle. Without NS309, the conformation of F410 cannot be determined. (*C*) Structure of the entire 2 × 2 CaM–CaMBD2-a complex in the presence of NS309. The structure model has the same view angle as in Fig. 1*B*. The most noticeable difference between this structure and that of Fig. 1*B* is the appearance of the well-defined IDF structure. (*D*) The F410L mutation reduces the modulatory effects of NS309. Values in parentheses indicate the number of experiments.

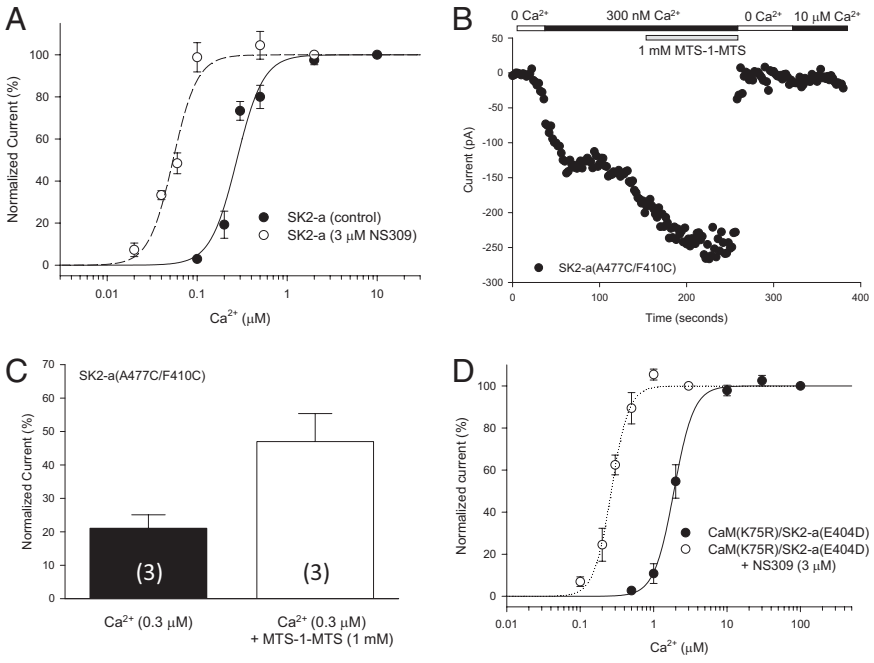

Fig. 4. The IDF on Ca^{2+}-dependent activation of SK channels. (*A*) NS309 increases the open probability of SK2 at a given Ca^{2+} concentration. Dose–response curves of Ca^{2+}-dependent activation of SK2-a were obtained with or without 3 μM NS309 in the bath solution. (*B*) Application of the cross-linker MTS-1-MTS (1 mM) doubles the current size of the same patch in the presence of 300 nM Ca^{2+}. After the bath solution was switched to 0 Ca^{2+}, subsequent application of 10 μM Ca^{2+} no longer could activate the channels modified by MTS-1-MTS, indicating that cross-linking has changed the structure of the IDF of the SK channels irreversibly. (*C*) Cross-linking A477C of the CaMBD and F410C of the IDF mimics the effect of NS309. The membrane patches expressing A477C/F410C were perfused sequentially with a solution of 10 μM Ca^{2+}, 300 nM Ca^{2+}, and 300 nM Ca^{2+} plus 1 mM MTS-1-MTS. The current amplitudes were normalized to that at 10 μM Ca^{2+}. Values in parentheses indicate the number of experiments. (*D*) Effects of mutations on the salt bridge between K75 of CaM and E404 of the IDF. The mutant pair K75R:E404D was able to rescue activation of the mutant channel by Ca^{2+}. NS309 is able to potentiate the Ca^{2+}-dependent activation of the mutant pair.

NS309 does not increase the current amplitude further once the channel activation has reached the maximal by Ca^{2+} (at 10 μM; Fig. S5*A*), indicating that NS309 does not activate SK/IK channels directly. The appearance of the IDF structure by NS309 (e.g., Fig. 3*C*) led us to postulate that binding of NS309 to the protein complex and its interaction with F410 might constrain the freedom of the IDF and result in a transition of an unstructured IDF to a well-defined conformation and, consequently, potentiation of the channel activity. We sought to test this hypothesis by cross-linking F410 of the IDF and A477 of the CaMBD, two residues known to interact with NS309 (Fig. 3*A*).

A cysteine residue was introduced at positions 410 and 477 of SK2-a. F410C/A477C activates in response to Ca^{2+} with a slightly reduced sensitivity ($EC_{50} = 0.45 \pm 0.06$ μM, $n = 4$, $P = 0.046$) (Fig. S5*B*), caused primarily by the F410C mutation ($EC_{50} = 0.51 \pm 0.02$ μM, $n = 3$). The patch membrane expressing F410C/A477C was exposed sequentially to solutions of 10 μM Ca^{2+} to achieve the maximal channel activation followed by 0.3 μM Ca^{2+} and 0.3 μM Ca^{2+} with 1 mM 1,1-methanediyl bismethanethiosulfonate (MTS-1-MTS). After the effect had reached steady state, the current amplitudes at each solution were normalized to that of 10 μM Ca^{2+}. Cross-linking by MTS-1-MTS significantly increases the current amplitude of F410C/A477C at 0.3 μM Ca^{2+} (Fig. 4*B*), with the normalized current more than doubled, from 21.1 ± 4.03% (before MST-1-MTS) to 47.0 ± 8.38% (after MTS-1-MTS; $n = 3$, $P = 0.036$, paired *t*-test) (Fig. 4*C*). Application of MTS-1-MTS to WT SK2-a or to the single point mutations F410C or A477C showed little change in Ca^{2+}-dependent channel activation (Fig. S5 *C–F*). Thus, cross-linking M410 of the IDF and A477 of the CaMBD by MTS-1-MTS can mimic the effect of NS309, but, unlike NS309, the effect of such cross-linking is irreversible (Fig. 4*B*).

We next sought to determine the potential impact of the salt bridge formed between E404 of the IDF and K75 of the CaM linker (Fig. S4*A*) on Ca^{2+}-dependent activation of SK channels. The interaction between E404 of the IDF and K75 of CaM is very sensitive to mutations, such as E404A, E404C, and K75C, which did not produce any measurable currents when expressed with their WT partners at Ca^{2+} concentrations as high as 100 μM. Even the very conservative mutations E404D and K75R failed to respond to Ca^{2+} when expressed individually with WT CaM or SK2-a. However, when E404D is coexpressed with K75R, the mutant pair becomes responsive to Ca^{2+} for its activation with reduced Ca^{2+} sensitivity ($EC_{50} = 1.96 \pm 0.18$, $n = 5$) compared with the WT pair (Fig. 4*D*; $P < 0.001$). NS309 (3 μM) significantly enhances the Ca^{2+}-dependent channel activation of the mutant pair ($EC_{50} = 0.27 \pm 0.02$ μM, $n = 4$, $P < 0.001$) (Fig. 4*D*; compare with Fig. 4*A*), indicating that E404D and K75R did express and that mutations have little impact on the ability of NS309 to increase the channel open probability. Collectively, the results suggest that the interaction between K75 of CaM and E404 of the IDF is critical for activation of SK channels by Ca^{2+}.

IDF in Coupling Ca^{2+}-Sensing and Channel Opening. We next addressed whether the IDF, at its different conformations, might impact the affinity of CaM for Ca^{2+}, resulting in changes in Ca^{2+}-dependent channel activation by different mutants or by NS309. A simple gating scheme shows that the apparent changes in Ca^{2+}-dependent activation of SK channels may result from changes of the affinity of CaM for Ca^{2+} and/or changes in coupling of Ca^{2+} binding to CaM and channel opening (Fig. S6*A*). Ca^{2+}-dependent interactions between CaM and the CaMBD2-a were measured using fluorophore-labeled CaM(T34C), as we previously described (14). The CaMBD2-a, with or without R396–M412 (Fig. S6 *B* and *C*), shows the same Ca^{2+}-dependent formation of the CaM–CaMBD-a complex (the apparent affinity for $Ca^{2+} = 0.28 \pm 0.01$ μM vs. 0.30 ± 0.03 μM, $n = 3$) (Fig. 5*A*), suggesting that the IDF does not directly alter the affinity of CaM for Ca^{2+}. No changes in the apparent Ca^{2+} affinity for formation of the CaM–CaMBD2-a complex are observed using CaM(T79D) or in the presence of saturating amount of NS309 ($EC_{50} = 0.32 \pm 0.03$ μM vs. 0.26 ± 0.02 μM, $n = 3$) (Fig. 5*A*). This finding is in contrast to our previous report, which shows that the reduced sensitivity for Ca^{2+}-dependent activation of SK2-b, an SK2 splice variant, is caused primarily by the reduced affinity of CaM for Ca^{2+} (14). Thus, we conclude that the primary role of the IDF is to couple binding of Ca^{2+} to CaM for mechanical opening of the channel pore. The conclusion is consistent with the structural data which show that Ca^{2+}-dependent formation of the CaM–CaMBD complex, as a consequence of binding of Ca^{2+} to CaM, must take place before the channel cuff can interact with the CaM linker (Figs. 1B and 3C) (14, 36, 37).

Discussion

In this study, we have demonstrated that an intrinsically disordered SK channel fragment (the IDF), which connects S6 and the CaMBD (Fig. 1*A*), plays a unique role in Ca^{2+}-dependent

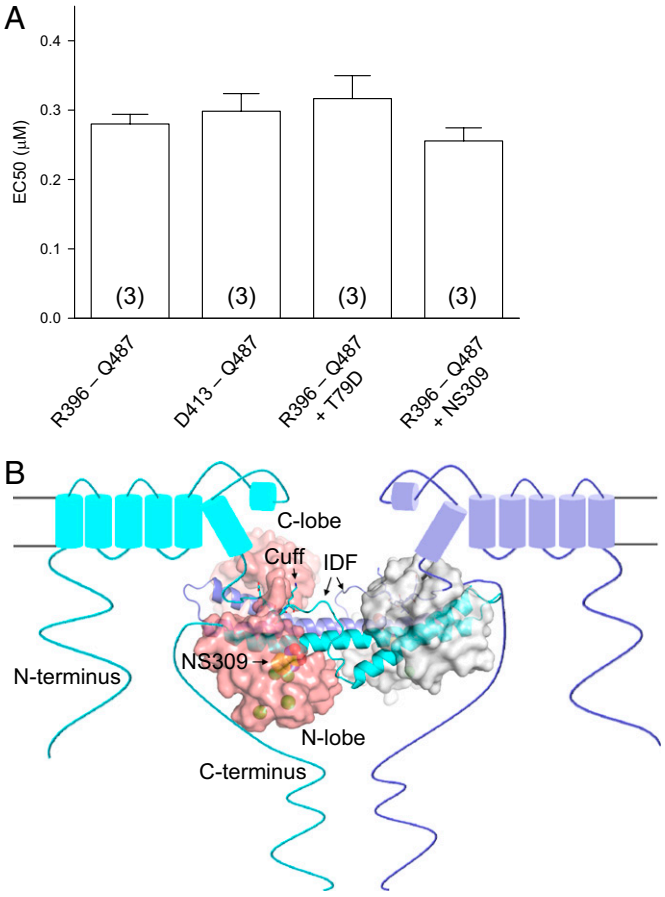

Fig. 5. The IDF does not alter the affinity of CaM for Ca^{2+}. (*A*) Effects of the IDF, NS309, or T79D on the Ca^{2+}-dependent formation of the CaM–CaMBD2-a complex. Fluorophore-labeled CaM(T34C) was mixed with channel peptides R396–Q487 (cuff + IDF + CaMBD2-a) or D413–Q487 (CaMBD) at different Ca^{2+} concentrations. A CaM mutant, CaM(T34C/T79D), or NS309 (saturating) also was used for the binding assays as indicated. No changes were seen in the apparent affinity for Ca^{2+} in Ca^{2+}-dependent formation of the CaM–CaMBD2-a complex under these manipulations. Values in parentheses indicate the number of experiments. (*B*) Structural model depicting the location of the CaM–CaMBD complex and the appearance of the IDF by NS309. Because of the interaction between the channel cuff and the CaM linker, the CaM–CaMBD complex is located much closer to the plasma membrane than previously thought. The unique conformation of the IDF, induced by NS309, couples the Ca^{2+} binding to CaM and the mechanical opening of the channel pore and increases the channel open probability at a given Ca^{2+} concentration.

activation of SK channels. Several lines of evidence support this conclusion. First, the IDF is highly conserved in its primary amino acid sequence, a characteristic of ID proteins/peptides (7). Second, the presence of NS309, the most potent channel modulator, has led to the transition of the unstructured IDF to a well-defined conformation. Because both ends of the IDF are anchored to CaM, such conformational changes are likely to occur and account for the action of NS309 in its potentiation of SK channel activities. Furthermore, such conformational changes coincide with increased channel open probability by NS309. Third, based on the structural data, cross-linking of F410 of the IDF and A477 of the CaMBD can increase the channel open probability at a given Ca^{2+} concentration, mimicking the effect of NS309. Finally, the IDF does not alter the affinity of CaM for Ca^{2+}. Our results also provide a structural basis for the greater potency of NS309 as compared with other compounds targeting SK/IK channels.

For a typical K^+ channel, S6 is part of the gate that controls the opening and closing of the channel pore (1, 2). The region immediately after S6 is proposed to have an important role in the gating mechanism(s) for ligand-gated K^+ channels, such as cyclic nucleotide-gated channels (1, 45–50). Our results provide direct structural and functional evidence that the IDF, highly conserved and located immediately after S6 (Fig. 5*B*), plays a key role in coupling the binding of Ca^{2+} to CaM and the mechanical opening of SK channels. Even though the structural data do not contain the entire channel, the interaction between the channel cuff and the CaM linker, confirmed by mutant cycle analysis of the full-length SK2 channel and CaM, shows that both the N and C termini of the IDF are anchored to CaM (Figs. 2*B* and 3*C*). Therefore, the conformation (or lack of conformation) of the IDF (compare Figs. 2*B* and 3*C*) is not caused by the absence of the entire channel in our structural data. Our results also show that the interactions between CaM and the channel for Ca^{2+}-dependent activation are much more extensive than previously thought (14, 36, 37). In particular, the interactions near the CaM linker contribute directly to the mechanical opening of the SK channel after Ca^{2+} is bound to CaM. Furthermore, the interaction between the channel cuff and the CaM linker suggests that the entire CaM complex is located immediately after S6 and very close to the plasma membrane (Fig. 5*B*). The results also provide a mechanistic explanation for the observation that phosphorylation of CaM T79 by protein kinase CK2 reduces the sensitivity of SK channels to Ca^{2+} by interfering with the mechanical coupling process rather than with Ca^{2+} binding to CaM, as previously suggested (51). Regulation of the interaction between the channel cuff and CaM linker by CK2 contributes directly to regulation of the membrane excitability by neurotransmitters (52).

Although significant strides have been made in development of small molecules targeting SK/IK channels (15, 28–32), knowledge is lacking regarding the binding site for these compounds, and very little is known about how these compounds achieve their potency. In our previous report, we showed, by molecular docking, that NS309, the most potent compound, seems to be much more potent than predicted based on the calculated binding energy (ΔG) of NS309 for the binding site of phenylurea (PHU) (44). PHU is ∼4,000-fold less potent than NS309 in potentiating SK/IK channel activities. We speculated that the NS309 binding site might have distinct structural features, because a previous report suggested that NS309 may achieve its effect by stabilizing the CaM–CaMBD complex (34). Indeed, the NS309-bound structure shows that the NS309 binding site has its own unique structural properties, in particular the appearance of the conformation of the IDF, even though the NS309 binding site shares the same general location with that of PHU or 1-EBIO (Fig. 3 and Fig. S4). The two weaker compounds, PHU and 1-EBIO, fail to stabilize the conformation of the IDF (44).

ID proteins often adopt different conformations, which cannot be determined by conventional methods such as X-ray crystallography (3–5). Our results provide a rare example showing that the presence of NS309, the most potent channel modulator (38, 39), can constrain the freedom of the IDF and turn the unstructured IDF into a well-defined conformation (Fig. 5*B*). The transition from an unstructured to well-structured IDF, by NS309, correlates with the increased channel open probability by NS309. This conclusion is corroborated by experiments, such as mutations or cross-linking F410 of the IDF and A477 of the CaMBD by MTS-1-MTS on the full-length channel (Fig. 4). Therefore, our results provide direct evidence that NS309 can stabilize the conformation of the CaM–SK complex, which favors channel opening, and achieve its high potency (34). Compounds targeting SK/IK channels are known to be beneficial in disorders of the central nervous system and the cardiovascular system (27, 53). Thus, our results provide a rationale for the development of small-molecule compounds targeting the ID protein/regions (3, 40).

Methods

Protein Crystallization and Structure Determination. Details of protein expression, purification, and crystallization can be found in our previous reports (14, 44). Briefly, the cDNA fragment encoding the C-terminal fragment (R395–Q486) of a rat SK2 channel (SK2-a, GenBank accession number

NM_019314) was cloned into pET-28b for protein expression, as was the rat CaM cDNA (GenBank accession number NM_012518). Both were expressed in *Escherichia coli* and purified to homogeneity. The channel fragment has a polyhistidine tag at its C terminal end. Crystals of the protein complex were grown in either sitting or hanging drops by vapor diffusion at 20 °C (14, 37). Because of the poor water solubility of NS309, the preformed protein crystals were incubated with NS309 at its saturating concentration, for 4–7 months before diffraction data were collected for the NS309-bound CaM complexes.

Electrophysiology. Both SK2-a (WT or mutants) and CaM (WT or mutants) along with GFP at a ratio of 5:2.5:1 (wt/wt/wt), were expressed in TsA201 cells (14, 44). Channel activities were recorded 1–2 d after transfection, using an insideout patch configuration at room temperature. The pipette solution contained (in mM): 140 KCl, 10 Hepes, 1 MgSO4 (pH 7.4). The bath solution contained (in mM): 140 KCl and 10 Hepes (pH 7.2). EGTA (1 mM), DibromoBATA (0.1 mM), and HEDTA (1 mM) were mixed with Ca2+ to obtain desired free Ca2+ concentrations. Currents were recorded by repetitive 1-s voltage ramps from −100 mV to +100 mV from a holding potential of 0 mV.

Additional details of methods can be found in *Supporting Information*.

Statistical Analysis. Unless stated, all data are presented as mean ± SEM, and the Student's *t*-test or paired *t*-test was used for data comparison.

ACKNOWLEDGMENTS. We thank Drs. Spike Horn, Pat Loll, Steve Siegelbaum, Jianmin Cui, and Zhe Lu and Mr. Warren Anderson for encouragement and helpful discussions at different stages of this work; the structural facility of the Kimmel Cancer Center of Thomas Jefferson University for access to equipment for initial protein crystal screening and initial in-house X-ray diffraction; and the staff at the Beamline facility (X29A and X6A) of the Brookhaven National Laboratory and the Structurally Integrated Biology for Life Sciences (SYBILS) Beamline 12.3.1 at the Advanced Light Source (Berkeley, CA) for assistance with collection of X-ray diffraction data. Use of the National Synchrotron Light Source at the Brookhaven National Laboratory was supported by the Office of Basic Energy Sciences, Office of Science, US Department of Energy under Contract DE-AC02-98CH10886. This work was supported by Grants R01MH073060 and R01NS39355 from the National Institutes of Health (to J.-F.Z.).

1. Yellen G (2002) The voltage-gated potassium channels and their relatives. *Nature* 419(6902):35–42.
2. Long SB, Tao X, Campbell EB, MacKinnon R (2007) Atomic structure of a voltage-dependent K^+ channel in a lipid membrane-like environment. *Nature* 450(7168): 376–382.
3. Babu MM, van der Lee R, de Groot NS, Gsponer J (2011) Intrinsically disordered proteins: Regulation and disease. *Curr Opin Struct Biol* 21(3):432–440.
4. Fuxreiter M, Simon I, Bondos S (2011) Dynamic protein-DNA recognition: Beyond what can be seen. *Trends Biochem Sci* 36(8):415–423.
5. Wang Y, et al. (2011) Intrinsic disorder mediates the diverse regulatory functions of the Cdk inhibitor p21. *Nat Chem Biol* 7(4):214–221.
6. Sugase K, Dyson HJ, Wright PE (2007) Mechanism of coupled folding and binding of an intrinsically disordered protein. *Nature* 447(7147):1021–1025.
7. Dyson HJ, Wright PE (2005) Intrinsically unstructured proteins and their functions. *Nat Rev Mol Cell Biol* 6(3):197–208.
8. Galea CA, et al. (2008) Role of intrinsic flexibility in signal transduction mediated by the cell cycle regulator, p27 Kip1. *J Mol Biol* 376(3):827–838.
9. Köhler M, et al. (1996) Small-conductance, calcium-activated potassium channels from mammalian brain. *Science* 273(5282):1709–1714.
10. Faber ESL, Sah P (2007) Functions of SK channels in central neurons. *Clin Exp Pharmacol Physiol* 34(10):1077–1083.
11. Stocker M (2004) $Ca^{(2+)}$-activated K^+ channels: Molecular determinants and function of the SK family. *Nat Rev Neurosci* 5(10):758–770.
12. Xu Y, et al. (2003) Molecular identification and functional roles of a $Ca^{(2+)}$-activated K^+ channel in human and mouse hearts. *J Biol Chem* 278(49):49085–49094.
13. Adelman JP, Maylie J, Sah P (2012) Small-conductance Ca^{2+}-activated K^+ channels: Form and function. *Annu Rev Physiol* 74:245–269.
14. Zhang M, et al. (2012) Structural basis for calmodulin as a dynamic calcium sensor. *Structure* 20(5):911–923.
15. Pedarzani P, Stocker M (2008) Molecular and cellular basis of small—and intermediate-conductance, calcium-activated potassium channel function in the brain. *Cell Mol Life Sci* 65(20):3196–3217.
16. Ohtsuki G, Piochon C, Adelman JP, Hansel C (2012) SK2 channel modulation contributes to compartment-specific dendritic plasticity in cerebellar Purkinje cells. *Neuron* 75(1):108–120.
17. Marrelli SP, Eckmann MS, Hunte MS (2003) Role of endothelial intermediate conductance KCa channels in cerebral EDHF-mediated dilations. *Am J Physiol Heart Circ Physiol* 285(4):H1590–H1599.
18. Si H, et al. (2006) Impaired endothelium-derived hyperpolarizing factor-mediated dilations and increased blood pressure in mice deficient of the intermediate-conductance Ca^{2+}-activated K^+ channel. *Circ Res* 99(5):537–544.
19. McNeish AJ, Dora KA, Garland CJ (2005) Possible role for K^+ in endothelium-derived hyperpolarizing factor-linked dilatation in rat middle cerebral artery. *Stroke* 36(7): 1526–1532.
20. Brähler S, et al. (2009) Genetic deficit of SK3 and IK1 channels disrupts the endothelium-derived hyperpolarizing factor vasodilator pathway and causes hypertension. *Circulation* 119(17):2323–2332.
21. Garland CJ (2010) Compromised vascular endothelial cell SK(Ca) activity: A fundamental aspect of hypertension? *Br J Pharmacol* 160(4):833–835.
22. Köhler R (2010) Single-nucleotide polymorphisms in vascular Ca^{2+}-activated K^+-channel genes and cardiovascular disease. *Pflugers Arch* 460(2):343–351.
23. Allen D, et al. (2011) SK2 channels are neuroprotective for ischemia-induced neuronal cell death. *J Cereb Blood Flow Metab* 31(12):2302–2312.
24. Chou CC, Lunn CA, Murgolo NJ (2008) KCa3.1: Target and marker for cancer, autoimmune disorder and vascular inflammation? *Expert Rev Mol Diagn* 8(2):179–187.
25. Ellinor PT, et al. (2010) Common variants in KCNN3 are associated with lone atrial fibrillation. *Nat Genet* 42(3):240–244.
26. Hopf FW, et al. (2010) Reduced nucleus accumbens SK channel activity enhances alcohol seeking during abstinence. *Neuron* 65(5):682–694.
27. Kasumu AW, et al. (2012) Selective positive modulator of calcium-activated potassium channels exerts beneficial effects in a mouse model of spinocerebellar ataxia type 2. *Chem Biol* 19(10):1340–1353.
28. Girault A, et al. (2012) Targeting SKCa channels in cancer: Potential new therapeutic approaches. *Curr Med Chem* 19(5):697–713.
29. Blank T, Nijholt I, Kye M-J, Spiess J (2004) Small conductance Ca2+-activated K+ channels as targets of CNS drug development. *Curr Drug Targets CNS Neurol Disord* 3(3):161–167.
30. Liégeois JF, et al. (2003) Modulation of small conductance calcium-activated potassium (SK) channels: A new challenge in medicinal chemistry. *Curr Med Chem* 10(8): 625–647.
31. Wulff H, Zhorov BS (2008) K^+ channel modulators for the treatment of neurological disorders and autoimmune diseases. *Chem Rev* 108(5):1744–1773.
32. Wulff H, et al. (2000) Design of a potent and selective inhibitor of the intermediate-conductance Ca^{2+}-activated K^+ channel, IKCa1: A potential immunosuppressant. *Proc Natl Acad Sci USA* 97(14):8151–8156.
33. Xia XM, et al. (1998) Mechanism of calcium gating in small-conductance calcium-activated potassium channels. *Nature* 395(6701):503–507.
34. Li W, Halling DB, Hall AW, Aldrich RW (2009) EF hands at the N-lobe of calmodulin are required for both SK channel gating and stable SK-calmodulin interaction. *J Gen Physiol* 134(4):281–293.
35. Meador WE, Means AR, Quiocho FA (1992) Target enzyme recognition by calmodulin: 2.4 A structure of a calmodulin-peptide complex. *Science* 257(5074):1251–1255.
36. Schumacher MA, Crum M, Miller MC (2004) Crystal structures of apocalmodulin and an apocalmodulin/SK potassium channel gating domain complex. *Structure* 12(5): 849–860.
37. Schumacher MA, Rivard AF, Bächinger HP, Adelman JP (2001) Structure of the gating domain of a Ca^{2+}-activated K^+ channel complexed with Ca^{2+}/calmodulin. *Nature* 410(6832):1120–1124.
38. Strøbaek D, et al. (2004) Activation of human IK and SK Ca^{2+} -activated K^+ channels by NS309 (6,7-dichloro-1H-indole-2,3-dione 3-oxime). *Biochim Biophys Acta* 1665(1-2):1–5.
39. Pedarzani P, et al. (2005) Specific enhancement of SK channel activity selectively potentiates the afterhyperpolarizing current I(AHP) and modulates the firing properties of hippocampal pyramidal neurons. *J Biol Chem* 280(50):41404–41411.
40. Follis AV, Galea CA, Kriwacki RW (2012) Intrinsic protein flexibility in regulation of cell proliferation: Advantages for signaling and opportunities for novel therapeutics. *Adv Exp Med Biol* 725:27–49.
41. Yang N, George AL, Jr., Horn R (1996) Molecular basis of charge movement in voltage-gated sodium channels. *Neuron* 16(1):113–122.
42. Ranganathan R, Lewis JH, MacKinnon R (1996) Spatial localization of the K^+ channel selectivity filter by mutant cycle-based structure analysis. *Neuron* 16(1):131–139.
43. Hidalgo P, MacKinnon R (1995) Revealing the architecture of a K^+ channel pore through mutant cycles with a peptide inhibitor. *Science* 268(5208):307–310.
44. Zhang M, Pascal JM, Schumann M, Armen RS, Zhang JF (2012) Identification of the functional binding pocket for compounds targeting small-conductance Ca^{2+}-activated potassium channels. *Nat Commun* 3:1021.
45. Yang J, et al. (2010) An epilepsy/dyskinesia-associated mutation enhances BK channel activation by potentiating Ca^{2+} sensing. *Neuron* 66(6):871–883.
46. Clayton GM, Silverman WR, Heginbotham L, Morais-Cabral JH (2004) Structural basis of ligand activation in a cyclic nucleotide regulated potassium channel. *Cell* 119(5):615–627.
47. Craven KB, Zagotta WN (2006) CNG and HCN channels: Two peas, one pod. *Annu Rev Physiol* 68:375–401.
48. Fodor AA, Aldrich RW (2009) Convergent evolution of alternative splices at domain boundaries of the BK channel. *Annu Rev Physiol* 71:19–36.
49. Zhou L, Siegelbaum SA (2007) Gating of HCN channels by cyclic nucleotides: Residue contacts that underlie ligand binding, selectivity, and efficacy. *Structure* 15(6):655–670.
50. Brelidze TI, Carlson AE, Sankaran B, Zagotta WN (2012) Structure of the carboxy-terminal region of a KCNH channel. *Nature* 481(7382):530–533.
51. Bildl W, et al. (2004) Protein kinase CK2 is coassembled with small conductance $Ca^{(2+)}$-activated K^+ channels and regulates channel gating. *Neuron* 43(6):847–858.
52. Maingret F, et al. (2008) Neurotransmitter modulation of small-conductance Ca^{2+}-activated K^+ channels by regulation of Ca^{2+} gating. *Neuron* 59(3):439–449.
53. Nagy N, et al. (2011) Role of Ca^2+-sensitive K+ currents in controlling ventricular repolarization: Possible implications for future antiarrhytmic drug therapy. *Curr Med Chem* 18(24):3622–3639.

PHYSIOLOGY